Toward single particle reconstruction without particle picking: Breaking the detection limit

Tamir Bendory, Nicolas Boumal, William Leeb, Eitan Levin and Amit Singer

July 30, 2018

Abstract

Here comes the abstract

1 Introduction

[Revise–Cryo–electron microscopy (cryo–EM) is an innovative technology for single particle reconstruction (SPR) of macromolecules.] In a cryo–EM experiment, biological samples are rapidly frozen in a thin layer of vitreous ice. Within the ice, the molecules are randomly oriented and positioned. The microscope produces a 2-D tomographic image of the samples embedded in the ice, called a *micrograph*. Each micrograph contains tomographic projections of the samples at unknown locations and under unknown viewing directions. The goal is to construct 3-D models of the molecules from the micrographs.

The signal to noise ratio (SNR) of the projections in the micrographs is a function of two dominating factors. On the one hand, the SNR is a function of the electron dose. To keep radiation damage within acceptable bounds, the dose must be kept low, which leads to high noise levels. On the other hand, the SNR is a function of the molecule [size/weight]. The smaller the molecules, the fewer detected electrons carry information about them.

All contemporary methods in the field split the reconstruction procedure into several stages. The first stage consists in extracting the various particle projections from the micrographs. This stage is called *particle picking*. Later stages aim to construct a 3-D model of the molecule from these projections. The quality of the reconstruction eventually hinges on the quality of the particle picking stage. Figure 1 illustrates how particle picking becomes increasingly challenging as the SNR degrades.

Crucially, it can be shown that reliable detection of individual particles is impossible below a certain critical SNR; see for instance [1][To verify the title]. This fact has been recognized early on by the cryo-EM community. In particular, in an influential paper from 1995, Henderson [8] investigates the following questions:

> For the purposes of this review, I would like to ask the question: what is the smallest size of free-standing molecule whose structure can in principle be determined by phase-contrast electron microscopy? Given what has already been demonstrated in published work, this reduces to the question: what is the smallest size of molecule for which it is possible to determine from images of unstained molecules the five

> *parameters needed to define accurately its orientation (three parameters) and position (two parameters) so that averaging can be performed?*

In that paper and in others that followed (e.g., [5]), it was established that particle picking is impossible for molecules below a certain weight (below ∼50 kDa). Joachim Frank voices a similar observation in his Nobel prize lecture: "*Using the ribosome as an example, it became clear from the formula we obtained that the single-particle approach to structure research was indeed feasible for molecules of sufficient size: Particle Size > 3/[Contrast² × Resolution (as length) × Critical Electron Dose]*" [4]. [As these two leaders of the cryo-EM community point out,] it is impossible to reconstruct small molecules by any of the existing computational pipelines for single particle analysis in cryo–EM, because the particles themselves cannot be picked from the micrographs.

The unique issues raised by small particles have been mitigated by recent technological advances in the field, including the use of Volta phase plates [10, 13] and scaffolding cages [14]. Despite this progress, detecting small molecules in the micrographs remains a challenge. We note that nuclear magnetic resonance (NMR) spectroscopy and X-ray crystallography are well suited to reconstruct small molecules. Yet, cryo–EM has a lot to offer even for molecules with already known structures obtained via NMR spectroscopy or X-ray crystallography, because these methods have limited ability to distinguish conformational variability. [Need a ref for this claim.]

In this paper, we argue that there is a gap between the two questions in Henderson's quoted excerpt above, and that one may be able to exploit it to design better reconstruction algorithms. Specifically, the impossibility of particle picking does not necessarily imply impossibility of particle reconstruction. Indeed, the aim is only to reconstruct the molecule: estimating the locations of the particles in the micrograph is merely a helpful intermediate stage when it can be done. Our main message is that the limits particle picking imposes on molecule size do not translate into limits on particle reconstruction.

As a proof of concept, we study a simplified model for 3-D reconstruction directly from the micrograph on a simulated data. In order to recover the 3-D volume, we use autocorrelation analysis. In a nutshell, we relate the autocorrelations of the micrographs to the autocorrelations of the volume. For any noise level, these autocorrelations can be estimated to any desired accuracy, provided the we get to observe sufficiently many particle projections and the latter are separated in the micrograph. Importantly, there is no need to detect the projections. The autocorrelations of the micrographs are straightforward to compute and require only one pass over the data. These directly yield estimates for the autocorrelations of the volume. To estimate the volume itself from its estimated autocorrelations, we solve a nonlinear inverse problem via least-squares. In this controlled experiment, we make several simplified assumptions; see the Discussion Section for details. As a side note, we mention that expectation-maximization (EM)—a popular framework in SPR—is intractable for this problem; see [1] for the details. [Do we want to stress that we get only low-resolution of the volume?]

Another interesting feature of the described approach pertains to model bias, whose importance in cryo-EM was stressed by a number of authors [17, 19, 9, 18]. In the classical "Einstein from noise" experiment, multiple realizations of pure noise are aligned to a picture of Einstein using template matching and then averaged. In [17], it was shown that the averaged noise rapidly becomes remarkably similar to the Einstein template. In the context of

(a) $\sigma = 0$ (b) $\sigma = 0.5$ (c) $\sigma = 3$

Figure 1: ⌈Example of micrographs of size 250×250 with additive white Gaussian noise of variance σ^2 for increasing values of σ. Each micrograph contains the same four occurrences of a 50×50 image of Einstein. In panel (c), the noise level is such that it is very challenging to locate the occurrences of the planted image. In fact, it can be shown that at low SNR, reliable detection of individual image occurrences is impossible, even if the true image is known. By analogy to cryo-EM, this depicts a scenario where particle picking cannot be done. [Do we want to replace with a cryo-EM figure?]

cryo–EM, this experiment exemplifies how prior assumptions about the particles may influence the reconstructed structure. This model bias is common to all particle picking methods based on template matching. In our approach, no templates are required, thus significantly reducing concerns about model bias. [To add reference to our example.]

To illustrate the possibility to estimate a signal without detecting its locations, we first discuss a toy model for which it is easier to convey the mathematical principles. In this toy model, an unknown image appears numerous times at unknown locations in several micrographs, each affected by additive Gaussian noise—see Figure TKTK for an illustration. The goal is to estimate the planted image. The task is interesting in particular when the SNR is low enough that particle picking cannot be done reliably. This problem is interesting of its own as it appears in other scientific applications, such as spike sorting [12], passive radar [6] and system identification [15]. We study it in more details, including an extension to multiple planted images, in a companion paper [1].

2   Results

The techniques we advocate allow to recover a signal hidden in noisy micrographs without (even implicitly) detecting the location of signal repetitions in these micrographs. To illustrate the underlying principles of the method, it is instructive to start with a toy model where the target signal is an unknown 2-D image. The latter appears several times in noisy micrographs, at unknown locations. Toward recovery, we first compute the second-order autocorrelation of the micrographs. We then establish that the autocorrelation of the target image can be recovered from the autocorrelation of the micrographs in a straightforward manner. The more micrographs we collect, the more accurate the estimate of the image's autocorrelation. The target image is then estimated from its autocorrelation using a standard inversion algorithm

3

(up to elementary symmetries). The same principles carry over to the more challenging task of 3-D reconstruction from micrographs. The Methods Section provides additional details.

In the experiment, we estimated Einstein's image of size 50×50 and mean zero from a growing number of micrographs, each of size 4096×4096 pixels. A micrograph contains, on average, 700 occurrences of the target image at random locations. Thus, about 10% of each micrograph contains signal. The micrographs are contaminated with additive white Gaussian noise with standard deviation $\sigma = 3$ (this corresponds to $\mathsf{SNR} = 1/20$). This high noise level is illustrated in TKTK. To simplify the experiment, we assume the number of signal occurrences and the noise standard deviation are known. Micrographs are generated such that any two occurrences are always separated by at least 49 pixels in each direction. The separation restriction is discussed in more details in the Methods Section.

We compute the average second-order autocorrelation of the micrographs. This is a particularly simple computation which can be efficiently executed with a fast Fourier transform (FFT) on GPUs. In the Methods Section, we show how, owing to separation of the occurrences, a determined portion of the averaged autocorrelation allows to estimate the autocorrelation of the unknown image itself. Mathematically, it can be shown that for any noise level, the quality of this estimate improves steadily as the amount of data grows [1]. Then, to estimate the target image, we resort to a standard phase retrieval algorithm called relaxed-reflect-reflect (RRR) [3], initialized randomly.

Figure 2 shows several estimated images for a growing number of micrographs, and a movie is available in [supplementary material]. Figure 3 presents the normalized recovery error as a function of the amount of data available. Error is measured as the ratio of the root mean square error (RMSE) to the norm of the ground truth (square root of the sum of squared pixel intensities.) This is computed after fixing elementary symmetries (see Methods.) As evidenced by these figures, the ground truth image can be estimated increasingly well from increasingly many micrographs, without particle picking. [Tamir: I will rewrite it with the new experiment.] [Here the cryo-EM setup shows up]

4
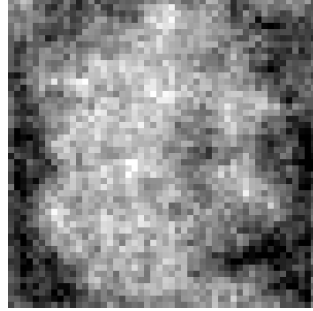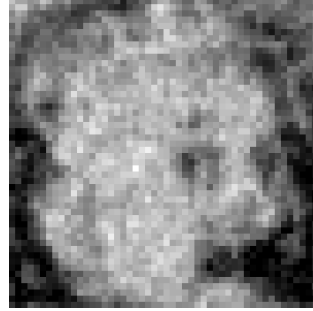
(a) $P = 512$ (b) $P = 512 \times 10$
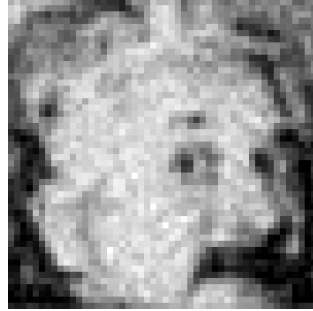
(c) $P = 512 \times 10^2$ (d) $P = 512 \times 10^3$

fig:Einst_example

Figure 2: Recovery of Einstein from micrographs at noise level $\sigma = 3$ (see Figure 1(c)). Averaged autocorrelations of the micrographs allow to estimate the power spectrum of the target image. This does not require particle picking. A phase retrieval algorithm (RRR) produces the estimates here shown, initialized with an image of the physicist Isaac Newton. Estimates are obtained from P micrographs (growing across panels), each containing 700 image occurrences on average. [To add: redo the figures according to Amit's comments and the figures of noisy Einstein's micrographs]
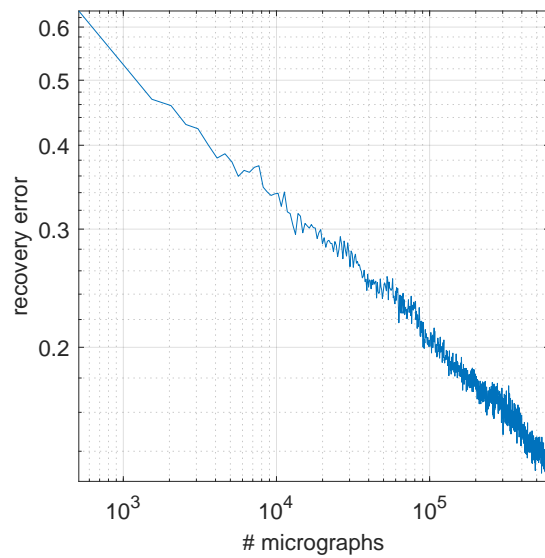
Figure 3: fig:error_per_micro Relative root mean square error of the estimate of Einstein's image as a function of the number of observed micrographs (logarithmic scale along both axes.)

3 Discussion

In the simplified model for cryo-EM we examined, we showed it is possible to estimate the 3-D structure of small volumes. Our strategy is to compute autocorrelation functions of the micrographs and to relate these statistics to the unknown volume's parameters. Recovering the parameters from the statistics reduces to solving a set of polynomial equations. Crucially, the outlined approach involves no particle picking, hence a fortiori no viewing direction estimation. Concerns for model bias are also greatly reduced since no template matching is involved.

Looking towards applying the framework to encompass all important features of real cryo-EM experiments, our work implies that it might be possible to reconstruct small molecules, in particular, molecules that are too small to be detected in micrographs. In pursuing this research direction, our goal is to significantly increase the range of molecules to which cryo-EM can be successfully applied. We recognize that significant challenges lay ahead for the implementation of the proposed approach to 3-D reconstruction directly from the micrographs. We discuss a few now.

[We should also incorporate Alberto's comment that our technique also allows to use much lower defocus values. Lower defocus means lower contrast, but will maintain higher frequency information. From that perspective, we may be able to get high resolution reconstructions from fewer micrographs, just because we would be using lower defocus.]

One possible concern is that the numerical experiments conducted here suggest a large amount of data may be necessary.[1] Recent trends in high-throughput cryo-EM technology [?] give hope that this may be a lesser concern in the long term. Still, large amounts of data also imply large amounts of computations. On this front, we note that computing autocorrelations can be executed efficiently on CPUs and GPUs, and in parallel across micrographs. It can even be done in streaming mode, as only one look at each micrograph is necessary. The output of this data processing stage is a succinct summary in the form of autocorrelation estimates: its size is a function of the resolution, not a function of the number of observed micrographs. Subsequent steps, which involve solving the system of polynomial equations, scale only in the size of that summary. Of course, an important question then is whether the equations can be solved meaningfully in practice. The proof-of-concept experiments above suggest they might.

Beyond data acquisition and computational challenges, there are modeling issues to consider. As stated, our approach relies on two core assumptions that are not necessarily verified in SPR experiments. First, we assume an additive white noise model, while in practice the noise may be correlated or signal dependent. To address this point, it may be necessary to investigate better noise models and to incorporate power spectrum estimation methods. Second, we assume that any two particles are sufficiently separated, and we use this assumption to derive algebraic relations between autocorrelations of the micrographs and autocorrelations of the 3-D volume. Perhaps this separation could be induced by careful experimental design [?]. Alternatively, if the signals are not well separated, one can introduce new parameters which encode the distribution of the spacing between occurrences. Here as well, relations between autocorrelations of the micrographs and of the volume could be derived.

We also note several aspects of SPR experiments that were neglected in this paper, in-

---

[1]Whether or not this large amount of data would be necessary for any method to succeed given the unfavorable SNR is an interesting research question.

cluding Contrast Transfer Function (CTF) correction and the non-uniformity of the viewing directions. All these aspects must be taken into account so the method could be applied on real data. We hope to take care of these issues in future research, as well to extend the proposed method to conformational heterogeneity. [another issue is that micrographs also contain contaminants such as carbon, ice crystals, etc..]

[Where and how do we cite Kam? Fred?]

4   Methods

4.1   Toy 2-D experiment

Let $x \in \mathbb{R}^{P \times P}$ be the target image and let $y \in \mathbb{R}^{N \times N}$ be one of K observed micrographs. Independently for each micrograph, the image formation model is as follows. An unknown binary signal $s \in \{0,1\}^{(N-P) \times (N-P)}$ indicates the starting positions of all occurrences of x in y, so that, with additive white Gaussian noise, we observe:

$$y = x * s + \varepsilon, \qquad\qquad \varepsilon \sim \mathcal{N}(0, \sigma^2 I), \qquad\qquad (4.1)$$

where $*$ denotes linear convolution, $\mathbf{i} := (i_1, i_2)$ identifies one location in the image and $\mathbf{i} = (0,0)$ indicates the upper left corner. We define the images to be zero outside their support. The binary signals s obey the following separation property:

If $s[\mathbf{i}] = 1$, then $s[\mathbf{j}] = 0$ for all $\mathbf{j} = (j_1, j_2)$ such that $\max\{|i_1 - j_1|, |i_2 - j_2|\} \le 2P - 1.$
$$(4.2)$$

In words: the upper left corners of any two occurrences of the target image x in a micrograph must be separated by at least $2P - 1$ pixels in each direction. Hence, each image is separated by a signal-free area that will ease the interpretation of the autocorrelation analysis. From the micrographs, we aim to recover x only. In this simplified model, we assume the total number of occurrences of the signal across micrographs is known. In the 3-D experiment we do not assume knowledge of the number of projections in the micrographs.

The second-order autocorrelation of an arbitrary image $z \in \mathbb{R}^{m \times m}$ is defined by

$$a_z^2[\boldsymbol{\ell}] = \frac{1}{N^2} \sum_{i_1 = \max\{0, -\ell_1\}}^{m-1+\min\{0, -\ell_1\}} \sum_{i_2 = \max\{0, -\ell_2\}}^{m-1+\min\{0, -\ell_2\}} z[\mathbf{i}] z[\mathbf{i} + \boldsymbol{\ell}]. \qquad (4.3)$$

Below, the image z might be either a target image x or the micrograph y. It can be shown that in the limit of infinitely many micrographs $K \to \infty$, the mean pixel value of the micrographs is equal to the mean pixel value of the signal x, scaled by

$$\gamma = \frac{MP^2}{N^2}, \qquad\qquad (4.4)$$

where M is the number of occurrences of x across micrographs. This is the fraction of entries of all micrographs occupied by occurrences of x, that is, the density of the signal. The spacing constraint (4.2) imposes $\gamma \le \frac{P}{2P-1} \approx 1/2$.

Similarly, numbering micrographs as $y_1, \ldots, y_K$, the empirical average of the second-order autocorrelations of the micrographs converges as follows:

$$\lim_{K \to \infty} \frac{1}{K} \sum_{k=1}^{K} a_{y_k}^2[\boldsymbol{\ell}] = \gamma a_x^2[\boldsymbol{\ell}] + \sigma^2 \delta_{(0,0)}[\boldsymbol{\ell}], \quad \boldsymbol{\ell} \in [0, P-1]^2, \tag{4.5}$$

{eq:a2}

where $\delta_{(i,j)}[\boldsymbol{\ell}] = 1$ for $\boldsymbol{\ell} = (i,j)$ and zero otherwise. Thus, for any noise level and without the need to even implicitly locate the images x in the micrographs, given sufficiently many micrographs we are able to compute the second-order autocorrelation of x itself. Recovering x from a_x^2 can be done up to symmetries, as detailed below. Equation (4.5) is proven and its extension to higher-order autocorrelations and multiple distinct planted images is discussed in [1].

For the 2-D experiment shown in Figures 2 and 3, we generate K micrographs of size 4096×4096 pixels. In each micrograph, we place Einstein's image (of zero mean) of size 50×50 in random locations, while preserving the separation condition (4.2). This is done by randomly selecting 4000 placements in the micrograph, one at a time with an accept/reject rule based on the separation constraint and locations picked so far. On average, 700 images are placed in each micrograph. Then, i.i.d. Gaussian noise with standard deviation $\sigma = 3$ is added, inducing an SNR of approximately $1/20$. An example of a micrograph's excerpt is presented in the right panel of Figure TKTK.

In this experiment, we assume γ and the noise level σ are known. In this setup, the second-order autocorrelation determines almost any target image uniquely, up to reflection through the origin [7]. The second-order autocorrelation can be computed at the cost of one 2-D FFT per micrograph. These can be computed highly efficiently and in parallel. To recover the image x itself, we use a standard algorithm used for phase retrieval called relaxed-reflect-reflect (RRR) [3].

In order to compare the performance in multiple cases and at different noise levels, the RRR is stopped after a fixed number of iterations (1000)[check] and the iterate with the smallest error compared to the ground truth (up to the reflection ambiguity) is chosen as the solution. While this cannot be done in practice (since we do not have access to the ground truth to determine which iterate is best), this procedure enables us to compare a large number of instances in different noise environments. [Note the last two sentences!] [Let's try with the last iterate and see]

4.2   3-D experiment

Let ϕ be the Coulomb potential representing the molecule we aim to recover. We assume that molecule is real-valued and smooth. In spherical coordinates, its 3-D Fourier transform $\widehat{\phi}$ admits a finite expansion of the form

$$\widehat{\phi}(k, \theta, \varphi) = \sum_{\ell=0}^{L} \sum_{m=-\ell}^{\ell} \sum_{s=1}^{S(\ell)} x_{\ell,m,s} Y_\ell^m(\theta, \varphi) j_{\ell,s}(k), \tag{4.6}$$

{eq:volume_expa

where Y_ℓ^m are complex spherical harmonics and $j_{\ell,s}$ are normalized spherical Bessel functions; see Appendix TKTK for further definitions. Let I_ω denote the tomographic projection obtained from viewing direction $\omega \in SO(3)$. By the Fourier projection-slice theorem, its 2-D

9

Fourier transform is given by [16]:

$$\widehat{I}_\omega(k,\varphi) = \sum_{\ell,m,m',s} x_{\ell,m,s} D^\ell_{m',m}(\omega) Y^{m'}_\ell \left(\frac{\pi}{2},\varphi\right) j_{\ell,s}(k), \qquad (4.7) \quad \{\text{eq:projection\_}$$

where $D^\ell_{m',m}(\omega)$ is a Wigner-D matrix.

Let $\mathcal{I} \in \mathbb{R}^{N \times N}$ denote a micrograph. We assume it consists of shifted copies of projections contaminated by additive white Gaussian noise:

$$\mathcal{I} = \sum_{t=1}^M I_{\omega_t} * \delta_{\mathbf{s}_t} + \varepsilon, \quad \varepsilon \sim \mathcal{N}(0,\sigma^2 I), \qquad (4.8) \quad \{\text{eq:micrograph\_}$$

where the viewing directions ω_t are assumed to be drawn from the uniform distribution over $SO(3)$ and $\mathbf{s}_t$ denotes the location of the center of the tth projection in the micrograph. Similarly to (4.2), we impose a separation condition so that any two projections are separated by at least $2P-1$ pixels between their upper left corners in each direction. Note that (4.1) can be also written as a sum of δ functions as in (4.8).

Define the pth autocorrelation of $\mathcal{I}$ as

$$a^p_\mathcal{I}(\boldsymbol{\ell}_1,\dots,\boldsymbol{\ell}_{p-1}) = \frac{1}{N^2} \sum_{\mathbf{i}} \mathcal{I}[\boldsymbol{\ell}] \mathcal{I}([\mathbf{i}+\boldsymbol{\ell}]_1) \cdots \mathcal{I}([\mathbf{i}+\boldsymbol{\ell}]_{p-1}),$$

where the summation is for $\mathbf{i}$ ranging over the N^2 pixels of the micrograph. Let $\mathcal{I}_1,\dots\mathcal{I}_K$ denote a set of K micrographs. Under the specified conditions, we show in Appendix A that the first three autocorrelations of the micrographs are related to those of the projections by

$$\lim_{K \to \infty} \frac{1}{K} \sum_{i=1}^K a^p_{\mathcal{I}_i}[\boldsymbol{\ell}_1,\dots,\boldsymbol{\ell}_{p-1}] = \gamma \left\langle a^p_{I_\omega}[\boldsymbol{\ell}_1,\dots,\boldsymbol{\ell}_{p-1}] \right\rangle_\omega + b_p[\boldsymbol{\ell}_1,\dots,\boldsymbol{\ell}_{p-1}], \qquad (4.9) \quad \{\text{eq:ac\_microgra}$$

$$p = 1,2,3, \quad \boldsymbol{\ell}_1,\dots,\boldsymbol{\ell}_{p-1} \in [-(P-1),P-1]^2,$$

where $\langle \cdot \rangle_\omega$ denotes averaging over all possible viewing directions ω and b_p is a bias term. Specifically, $b_1 = 0$ and therefore the mean is unbiased. The bias term of the second-order autocorrelation b_2 depends only on σ^2, the variance of the noise. Hence, if the noise level can be accurately estimated from the micrographs, this bias can be removed. Finally, the bias term of the third-order autocorrelation b_3 depends on the mean of the micrograph and σ^2. Therefore, given sufficiently many projections, we can accurately estimate the quantities $\gamma \langle a^p_{I_\omega} \rangle_\omega$ directly from the micrographs. These quantities are functions of the unknown coefficients $x_{l,m,s}$ and we could proceed to invert their relation, as we did in the 2-D toy example.

In practice, we want to leverage one more feature of the 3-D reconstruction problem. Since all in-plane rotations of the micrographs are equally likely observations, it is desirable in (4.9) to average over all in-plane rotations as well. This can be done efficiently using Prolate Spheroidal Wave Functions (PSWFs). We use autocorrelations up to and including the third order since this is necessary to determine the volume. The details are in the appendix.

Acknowledgment

Let's thank them all

References

[1] Tamir Bendory, Nicolas Boumal, William Leeb, Eitan Levin, and Amit Singer. Estimation below the detection limit with application to cryo-em. *preprint*, 2018.

[2] Tejal Bhamre, Teng Zhang, and Amit Singer. Denoising and covariance estimation of single particle cryo-em images. *Journal of structural biology*, 195(1):72–81, 2016.

[3] Veit Elser. Matrix product constraints by projection methods. *Journal of Global Optimization*, 68(2):329–355, 2017.

[4] Joachim Frank. Single-particle reconstruction of biological molecules-story in a sample (nobel lecture). *Angewandte Chemie International Edition*, 2018.

[5] Robert M Glaeser. Electron crystallography: present excitement, a nod to the past, anticipating the future. *Journal of structural biology*, 128(1):3–14, 1999.

[6] Sandeep Gogineni, Pawan Setlur, Muralidhar Rangaswamy, and Raj Rao Nadakuditi. Passive radar detection with noisy reference channel using principal subspace similarity. *IEEE Transactions on Aerospace and Electronic Systems*, 2017.

[7] MHMH Hayes. The reconstruction of a multidimensional sequence from the phase or magnitude of its fourier transform. *IEEE Transactions on Acoustics, Speech, and Signal Processing*, 30(2):140–154, 1982.

[8] Richard Henderson. The potential and limitations of neutrons, electrons and X-rays for atomic resolution microscopy of unstained biological molecules. *Quarterly reviews of biophysics*, 28(2):171–193, 1995.

[9] Richard Henderson. Avoiding the pitfalls of single particle cryo-electron microscopy: Einstein from noise. *Proceedings of the National Academy of Sciences*, 110(45):18037–18041, 2013.

[10] Maryam Khoshouei, Mazdak Radjainia, Wolfgang Baumeister, and Radostin Danev. Cryo-EM structure of haemoglobin at 3.2 å determined with the Volta phase plate. *Nature communications*, 8:16099, 2017.

[11] Boris Landa and Yoel Shkolnisky. Steerable principal components for space-frequency localized images. *SIAM journal on imaging sciences*, 10(2):508–534, 2017.

[12] Michael S Lewicki. A review of methods for spike sorting: the detection and classification of neural action potentials. *Network: Computation in Neural Systems*, 9(4):R53–R78, 1998.

[13] Yi-Lynn Liang, Maryam Khoshouei, Mazdak Radjainia, Yan Zhang, Alisa Glukhova, Jeffrey Tarrasch, David M Thal, Sebastian GB Furness, George Christopoulos, Thomas Coudrat, et al. Phase-plate cryo-EM structure of a class B GPCR–G-protein complex. *Nature*, 546(7656):118, 2017.

[14] Yuxi Liu, Shane Gonen, Tamir Gonen, and Todd O. Yeates. Near-atomic cryo-EM imaging of a small protein displayed on a designed scaffolding system. *Proceedings of the National Academy of Sciences*, 2018.

[15] Lennart Ljung. System identification. In *Signal analysis and prediction*, pages 163–173. Springer, 1998.

[16] Frank Natterer. *The mathematics of computerized tomography*, volume 32. SIAM, 1986.

[17] Maxim Shatsky, Richard J Hall, Steven E Brenner, and Robert M Glaeser. A method for the alignment of heterogeneous macromolecules from electron microscopy. *Journal of structural biology*, 166(1):67–78, 2009.

[18] Marin van Heel. Finding trimeric HIV-1 envelope glycoproteins in random noise. *Proceedings of the National Academy of Sciences*, 110(45):E4175–E4177, 2013.

[19] Marin van Heel, Michael Schatz, and Elena Orlova. Correlation functions revisited. *Ultramicroscopy*, 46(1–4):307–316, 1992.

[20] Zhizhen Zhao, Yoel Shkolnisky, and Amit Singer. Fast steerable principal component analysis. *IEEE transactions on computational imaging*, 2(1):1–12, 2016.

A Moments derivation

{sec:moment_de

In this section we prove relation (4.9). We note that mathematically taking infinitely many micrographs is equivalent to take one infinitely large micrograph with fixed density γ (4.4). Hence, we consider the moments of one micrograph $\mathcal{I}$ in the limit $N \to \infty$ and $\gamma = \lim_{N\to\infty} \frac{MP^2}{N^2} \in (0,1)$. The separation condition guarantees that if $\mathbf{i} = (i,j)$ is in the support of some projection, then $\mathbf{i} + \boldsymbol{\ell}$ for $\boldsymbol{\ell} \in [-(P-1), P-1]^2$ is either in the support of the same projection or outside the support of any projection.

We begin by calculating the relation between the pth autocorrelation of the clean micrograph and the averaged autocorrelation of the projections. Let us denote the clean micrograph by $\widetilde{\mathcal{I}} = \mathcal{I} - \varepsilon$, where $\mathcal{I}$ and ε are given in (4.8). Denote by $\mathcal{S}_t$ the support of the tth particle. Then, we have

$$
\begin{aligned}
a^p_{\widetilde{\mathcal{I}}}[\boldsymbol{\ell}_1, \ldots, \boldsymbol{\ell}_{p-1}] &= \frac{1}{N^2} \sum_{\mathbf{i}} \widetilde{\mathcal{I}}[\mathbf{i}]\widetilde{\mathcal{I}}[\mathbf{i}+\boldsymbol{\ell}_1] \cdots \widetilde{\mathcal{I}}[\mathbf{i}+\boldsymbol{\ell}_{p-1}] \\
&= \frac{1}{N^2} \sum_{t=1}^{M} \sum_{\mathbf{i} \in \mathcal{S}_t} \widetilde{\mathcal{I}}[\mathbf{i}]\widetilde{\mathcal{I}}[\mathbf{i}+\boldsymbol{\ell}_1] \cdots \widetilde{\mathcal{I}}[\mathbf{i}+\boldsymbol{\ell}_{p-1}] \\
&= \frac{MP^2}{N^2} \cdot \frac{1}{M} \sum_{t=1}^{M} \frac{1}{P^2} \sum_{i,j=0}^{P-1} I_{\omega_t}[\mathbf{i}]I_{\omega_t}[\mathbf{i}+\boldsymbol{\ell}_1] \cdots I_{\omega_t}[\mathbf{i}+\boldsymbol{\ell}_{p-1}] \\
&= \frac{MP^2}{N^2} \frac{1}{M} \sum_{t=1}^{M} a^p_{I_{\omega_t}}[\boldsymbol{\ell}_1, \ldots, \boldsymbol{\ell}_{p-1}] \\
&\to \gamma \langle a^p_{I_\omega}[\boldsymbol{\ell}_1, \ldots, \boldsymbol{\ell}_{p-1}]\rangle_\omega,
\end{aligned}
\tag{A.1}
$$

{eq:general_mo

where the average is taken over ω with respect to the distribution of viewing directions. Here, we assume it to be uniform.

In the presence of noise, we get additional bias terms denoted by b_p in (4.9). The mean ($p = 1$) is unbiased since the noise is assumed to have zero mean. For the second-order autocorrelation ($p = 2$), we have

$$
\begin{aligned}
a_{\mathcal{I}}^2[\boldsymbol{\ell}] &= \frac{1}{N^2} \sum_{\mathbf{i}} \mathcal{I}[\mathbf{i}]\mathcal{I}[\mathbf{i}+\boldsymbol{\ell}] \\
&= \frac{1}{N^2} \sum_{\mathbf{i}} \widetilde{\mathcal{I}}[\mathbf{i}]\widetilde{\mathcal{I}}[\mathbf{i}+\boldsymbol{\ell}] + \frac{1}{N^2} \sum_{\mathbf{i}} \widetilde{\mathcal{I}}[\mathbf{i}]\varepsilon[\mathbf{i}+\boldsymbol{\ell}] \\
&\quad + \frac{1}{N^2} \sum_{\mathbf{i}} \varepsilon[\mathbf{i}]\widetilde{\mathcal{I}}[\mathbf{i}+\boldsymbol{\ell}] + \frac{1}{N^2} \sum_{\mathbf{i}} \varepsilon[\mathbf{i}]\varepsilon[\mathbf{i}+\boldsymbol{\ell}].
\end{aligned}
$$

The first term is given by (A.1) for $p = 2$. The cross terms vanish in the limit. The fourth term is zero unless $\boldsymbol{\ell} = 0$, in which case it converges to σ^2. Thus, we conclude

$$
a_{\mathcal{I}}^2[\boldsymbol{\ell}] \to \gamma \langle a_{I_\omega}^2[\boldsymbol{\ell}] \rangle_\omega + \sigma^2 \delta[\boldsymbol{\ell}],
$$

where the bias term $b_2[\boldsymbol{\ell}] = \sigma^2 \delta[\boldsymbol{\ell}]$ depends only on the variance of the noise σ^2.

For the third moments, we get 8 terms:

$$
a_{\mathcal{I}}^3[\boldsymbol{\ell}_1, \boldsymbol{\ell}_2] = \underbrace{\frac{1}{N^2} \sum_{\mathbf{i}} \widetilde{\mathcal{I}}[\mathbf{i}]\widetilde{\mathcal{I}}[\mathbf{i}+\boldsymbol{\ell}_1]\widetilde{\mathcal{I}}[\mathbf{i}+\boldsymbol{\ell}_2]}_{(1)} + \underbrace{\frac{1}{N^2} \sum_{\mathbf{i}} \varepsilon[\mathbf{i}]\varepsilon[\mathbf{i}+\boldsymbol{\ell}_1]\varepsilon[\mathbf{i}+\boldsymbol{\ell}_2]}_{(2)}
$$

$$
+ \underbrace{\frac{1}{N^2} \sum_{\mathbf{i}} \widetilde{\mathcal{I}}[\mathbf{i}]\varepsilon[\mathbf{i}+\boldsymbol{\ell}_1]\widetilde{\mathcal{I}}[\mathbf{i}+\boldsymbol{\ell}_2]}_{(3)} + \underbrace{\frac{1}{N^2} \sum_{\mathbf{i}} \widetilde{\mathcal{I}}[\mathbf{i}]\widetilde{\mathcal{I}}[\mathbf{i}+\boldsymbol{\ell}_1]\varepsilon[\mathbf{i}+\boldsymbol{\ell}_2]}_{(4)}
$$

$$
+ \underbrace{\frac{1}{N^2} \sum_{\mathbf{i}} \varepsilon[\mathbf{i}]\widetilde{\mathcal{I}}[\mathbf{i}+\boldsymbol{\ell}_1]\widetilde{\mathcal{I}}[\mathbf{i}+\boldsymbol{\ell}_2]}_{(5)} + \underbrace{\frac{1}{N^2} \sum_{\mathbf{i}} \widetilde{\mathcal{I}}[\mathbf{i}]\varepsilon[\mathbf{i}+\boldsymbol{\ell}_1]\varepsilon[\mathbf{i}+\boldsymbol{\ell}_2]}_{(6)}
$$

$$
+ \underbrace{\frac{1}{N^2} \sum_{\mathbf{i}} \varepsilon[\mathbf{i}]\varepsilon[\mathbf{i}+\boldsymbol{\ell}_1]\widetilde{\mathcal{I}}[\mathbf{i}+\boldsymbol{\ell}_2]}_{(7)} + \underbrace{\frac{1}{N^2} \sum_{\mathbf{i}} \varepsilon[\mathbf{i}]\widetilde{\mathcal{I}}[\mathbf{i}+\boldsymbol{\ell}_1]\varepsilon[\mathbf{i}+\boldsymbol{\ell}_2]}_{(8)}.
$$

We address these terms one by one:

- Term (1) is treated by (A.1) for $p = 3$;

- Term (2) is the third-order autocorrelation of pure noise which vanishes in the limit;

- Terms (3)-(5) depend linearly on the noise and hence vanish in the limit;

- For term (6), if $\boldsymbol{\ell}_1 \neq \boldsymbol{\ell}_2$ the term vanishes in the limit. If $\boldsymbol{\ell}_1 = \boldsymbol{\ell}_2$ then

$$
\frac{1}{N^2} \sum_{\mathbf{i}} \widetilde{\mathcal{I}}[\mathbf{i}]\varepsilon[\mathbf{i}+\boldsymbol{\ell}]^2 = \frac{MP^2}{N^2} \cdot \frac{1}{MP^2} \sum_{t=1}^{M} \sum_{\mathbf{i} \in \mathcal{S}_t} I_{\omega_t}[\mathbf{i}]\varepsilon[\mathbf{i}+\boldsymbol{\ell}]^2 \to \gamma \sigma^2 \langle a_{I_\omega}^1 \rangle_\omega,
$$

where $\langle a_{I_\omega}^1 \rangle_\omega$ is the mean of the volume.

- Terms (7) and (8) contribute δ functions similar to (6).

Thus, we conclude that

$$a_{\mathcal{I}}^3[\boldsymbol{\ell}_1, \boldsymbol{\ell}_2] \to \gamma \langle a_{I_\omega}^3[\boldsymbol{\ell}_1, \boldsymbol{\ell}_2]\rangle_\omega + \gamma\sigma^2\langle a_{I_\omega}^1\rangle_\omega \Big(\delta[\boldsymbol{\ell}_1 - \boldsymbol{\ell}_2] + \delta[\boldsymbol{\ell}_1] + \delta[\boldsymbol{\ell}_2]\Big),$$

where the second term is the bias $b_3[\boldsymbol{\ell}_1, \boldsymbol{\ell}_2]$. Note that $\gamma\langle a_{I_\omega}^1\rangle_\omega$ is approximately the mean of the micrograph since $a_{\mathcal{I}}^1 \approx a_{\tilde{\mathcal{I}}}^1 \approx \gamma\langle a_{I_\omega}^1\rangle_\omega$. Therefore, we do not need prior knowledge of γ to effectively debias the third-order autocorrelation.

B   Accounting for all in-plane rotations

We represent our autocorrelations using Prolate Spheroidal Wave Functions (PSWFs) $\{\psi_{k,q}\}$ where $k \geq 0, q \geq 1$ are integers [11]. As we demonstrate below, this makes it easier to account for the fact that all in-plane rotations of the micrographs are equally likely observations. This is only a concern for the second and third order autocorrelations. Below, we start with $p = 2$. The PSWFs are eigenfunctions of the truncated Fourier transform and are given in polar coordinates by

$$\psi_{k,q}(r, \varphi) = \begin{cases} \frac{1}{\sqrt{8\pi}}\alpha_{k,q}R_{k,q}(r)e^{\iota k\varphi}, & r \leq 1, \\ 0, & r > 1, \end{cases} \tag{B.1}$$

where the $R_{k,q}$ are a family of real, one-dimensional functions and the $\alpha_{k,q}$ are [real?] scaling factors which will be defined in the next section. The PSWFs are orthonormal on the unit disk.

For $\boldsymbol{\ell} \in [-(P-1), P-1]^2$, let us define

$$\mathfrak{a}^2[k, q] = \sum_{\boldsymbol{\ell}} a_{\mathcal{I}}^2[\boldsymbol{\ell}]\overline{\psi_{k,q}[\boldsymbol{\ell}]},$$

where $\psi_{k,q}[\boldsymbol{\ell}] \triangleq \psi_{k,q}(\boldsymbol{\ell}/P)$ [?] is a discretization of the PSWFs. [Range of k, q? need approx orthonormality in discrete...] Knowledge of these coefficients is essentially equivalent to knowledge of the second-order correlations owing to the following approximate identity:

$$a_{\mathcal{I}}^2[\mathbf{i}] \approx \sum_{k,q} \mathfrak{a}^2[k, q]\psi_{k,q}[\boldsymbol{\ell}]. \tag{B.2}$$

We now proceed to show that the coefficients $\mathfrak{a}^2[k, q]$ can be computed from the micrographs directly.

By definition,

$$\begin{aligned} \mathfrak{a}^2[k, q] &= \sum_{\boldsymbol{\ell}} a_{\mathcal{I}}^2[\boldsymbol{\ell}]\overline{\psi_{k,q}[\boldsymbol{\ell}]} \\ &= \frac{1}{N^2}\sum_{\mathbf{i}} \mathcal{I}[\mathbf{i}]\left(\sum_{\boldsymbol{\ell}} \mathcal{I}[\mathbf{i} + \boldsymbol{\ell}]\overline{\psi_{k,q}[\boldsymbol{\ell}]}\right) \\ &= \frac{1}{N^2}\sum_{\mathbf{i}} \mathcal{I}[\mathbf{i}]a_{k,q}[\mathbf{i}], \end{aligned} \tag{B.3}$$

14

where we defined

$$a_{k,q}[\mathbf{i}] = \sum_{\boldsymbol{\ell}} \mathcal{I}[\mathbf{i}+\boldsymbol{\ell}]\overline{\psi_{k,q}[\boldsymbol{\ell}]}.$$

These coefficients can be computed efficiently. Indeed, consider a patch of the micrograph $\mathcal{I}$ centered around pixel $\mathbf{i}$ and of size $(2P-1) \times (2P-1)$. This is exactly the patch indexed in the sum above. Hence, using the same approximation as we did in (B.2), a direct expansion of that patch in the discretized PSWFs yields the sought coefficients:

$$\mathcal{I}[\mathbf{i}+\boldsymbol{\ell}] \approx \sum_{k,q} a_{k,q}[\mathbf{i}]\psi_{k,q}[\boldsymbol{\ell}]. \tag{B.4} \quad \texttt{\{eq:itamar\}}$$

Thus, we proceed as follows: for each position $\mathbf{i}$ in the micrograph $\mathcal{I}$, we extract the corresponding patch of size $2P-1$, expand it in the discretized PSWFs as in (B.4), and collect the $a_{k,q}$ as per (B.3) to constitute the second-order autocorrelation of the micrograph.

Crucially, following this formalism, it is now straightforward to account for all in-plane rotations (and reflections) of the micrograph. Indeed, as can be seen from the definition of the (continuous) PSWFs (B.1), the effects of rotations and reflections on expansion coefficients of real images are, respectively, phase modulation and conjugation. By analogy in the discrete case, we have the following approximate expansions for a patch rotated about its center $\mathbf{i}$ by an angle α:

$$\mathcal{I}^{\alpha,+}[\mathbf{i}+\boldsymbol{\ell}] = \sum_{k,q} a_{k,q}e^{-ik\alpha}\psi_{k,q}[\boldsymbol{\ell}],$$

and the reflection followed by a rotation by angle α:

$$\mathcal{I}^{\alpha,-}[\mathbf{i}+\boldsymbol{\ell}] = \sum_{k,q} \overline{a_{k,q}}e^{-ik\alpha}\psi_{k,q}[\boldsymbol{\ell}].$$

Averaging over all rotations of the patch $\mathcal{I}(\mathbf{i}+\Delta\mathbf{i})$ and its reflection we get

$$\begin{aligned}
\mathfrak{a}^2[k,q] &= \frac{1}{N^2}\sum_{\mathbf{i}} \mathcal{I}[\mathbf{i}]\left(\frac{1}{4\pi}\int_0^{2\pi}[a_{k,q}[\mathbf{i}] + \overline{a_{k,q}}[\mathbf{i}]]e^{-ik\alpha}\,d\alpha\right) \\
&= \delta[k]\frac{1}{N^2}\sum_{\mathbf{i}}\mathcal{I}[\mathbf{i}]a_{0,q}[\mathbf{i}],
\end{aligned}$$

where in the last equality we used that both $\mathcal{I}$ and $\psi_{0,q}$ are real valued. Thus, the second-order autocorrelation, though two-dimensional, effectively only provides one-dimensional information.

We now follow a similar approach to estimate the bias term b_2. Introduce the coefficients $\mathfrak{b}_2$ as: [We're using that R functions are zero at the origin for $k \neq 0$, right? We didn't introduce that fact so far.]

$$\begin{aligned}
\mathfrak{b}_2[k,q] &= \sigma^2\sum_{\boldsymbol{\ell}}\delta[\boldsymbol{\ell}]\overline{\psi_{k,q}[\boldsymbol{\ell}]} \\
&= \sigma^2\overline{\psi_{k,q}[\mathbf{0}]} \\
&= \delta[k]\frac{\sigma^2}{\sqrt{2\pi}}R_{0,q}(0).
\end{aligned}$$

15

With this definition, we have the usual approximation:

$$b_2[\boldsymbol{\ell}] = \sigma^2 \delta[\boldsymbol{\ell}] \approx \sum_{k,q} \mathfrak{b}_2[k,q] \psi_{k,q}[\boldsymbol{\ell}].$$

We then estimate the expansion coefficients of the clean power spectrum as

$$\widetilde{\mathfrak{m}_2}(k,q) = \mathfrak{m}_2(k,q) - \mathfrak{b}_2(k,q).$$

[—————————————————]
, which we use to include all in-plane rotations of the projections in the micrograph to compute the autocorrelations, and compute only the blocks on the diagonal - see . The PSWFs are eigenfunctions of the truncated Fourier transform and satisfy

$$\alpha_{k,q} \psi_{k,q}(\mathbf{k}) = \sum_{\mathbf{i}} \psi_{k,q}(\mathbf{i}) e^{-2\pi \iota (\mathbf{i} \cdot \mathbf{k})} \tag{B.5}$$ {eq:PSWF_defn_e

given in polar coordinates by

$$\psi_{k,q}(r, \varphi) = \begin{cases} \frac{1}{2\sqrt{2\pi}} \alpha_{k,q} R_{k,q}(r) e^{\iota k \varphi}, & r \leq 1, \\ 0, & r > 1, \end{cases} \quad k \geq 0, \ q \geq 1,$$

and are orthonormal on the unit disc.[2]

The micrograph autocorrelations are given by an average over the particle orientations. Since the specific in-plane rotation of each projection is equally likely to appear, we would like to consider all possible in-plane rotations. This can be done efficiently using steerable bases , a basis in which an in-plane rotation corresponds to a phase shift of the expansion coefficients; [2, 11, 20].

The clean autocorrelations $\gamma \langle m_k[I_\omega] \rangle_\omega$ which we estimate from the micrograph are given by an average over the particule orientations. In particular, they are invariant under in-plane rotations of the projections, and can therefore be block-diagonalized in any steerable basis, a basis in which an in-plane rotation corresponds to a phase shift of the expansion coefficients - see [2, 11, 20]. For this paper, we represent our autocorrelations using Prolate Spheroidal Wave Functions (PSWFs) $\{\psi_{k,q}\}$, which we use to include all in-plane rotations of the projections in the micrograph to compute the autocorrelations, and compute only the blocks on the diagonal - see [11].

The PSWFs are eigenfunctions of the truncated Fourier transform and satisfy [approximate] [generate the Gram matrix of the discrete approximation]

$$\alpha_{k,q} \psi_{k,q}(\mathbf{k}) = \sum_{\mathbf{i}} \psi_{k,q}(\mathbf{i}) e^{-2\pi \iota (\mathbf{i} \cdot \mathbf{k})} \tag{B.6}$$ {eq:PSWF_defn_e

given in polar coordinates by

$$\psi_{k,q}(r, \varphi) = \begin{cases} \frac{1}{2\sqrt{2\pi}} \alpha_{k,q} R_{k,q}(r) e^{\iota k \varphi}, & r \leq 1, \\ 0, & r > 1, \end{cases} \quad k \geq 0, \ q \geq 1,$$

---

[2]In [11], PSWFs are defined as $2\psi_{k,q}/\alpha_{k,q}$, but using the above definition simplifies the formula for the expansion coefficients.

and are orthonormal on the unit disc.[3]

The mean is a scalar and is already invariant under in-plane rotations of the projections in the dataset, since all projections have the same mean $Lm_1[\phi]$, as explained above. For the power spectrum, we expand it as

$$m_2[\mathcal{I}](\Delta\mathbf{i}) = \sum_{k,q} \mathfrak{m}_2(k,q)\psi_{k,q}(\Delta\mathbf{i}),$$

where the expansion is truncated according to the rule in [11], and obtain the expansion coefficients as

$$\mathfrak{m}_2(k,q) = \sum_{\Delta\mathbf{i}} m_2[\mathcal{I}](\Delta\mathbf{i})\overline{\psi_{k,q}(\Delta\mathbf{i})}$$

$$= \frac{1}{L^2}\sum_{\mathbf{i}}\mathcal{I}(\mathbf{i})\left(\sum_{\Delta\mathbf{i}}\mathcal{I}(\mathbf{i}+\Delta\mathbf{i})\overline{\psi_{k,q}(\Delta\mathbf{i})}\right)$$

$$= \frac{1}{L^2}\sum_{\mathbf{i}}\mathcal{I}(\mathbf{i})a_{k,q}(\mathbf{i}),$$

where we note that if we expand a patch of size $(2L-1)\times(2L-1)$ centered about $\mathcal{I}(\mathbf{i})$ in PSWFs as

$$\mathcal{I}(\mathbf{i}+\Delta\mathbf{i}) = \sum_{k,q} a_{k,q}(\mathbf{i})\psi_{k,q}(\Delta\mathbf{i}), \quad ||\Delta\mathbf{i}||_\infty \leq L-1,$$

the expansion coefficients are given by the inner product

$$a_{k,q}(\mathbf{i}) = \sum_{\Delta\mathbf{i}}\mathcal{I}(\mathbf{i}+\Delta\mathbf{i})\overline{\psi_{k,q}(\Delta\mathbf{i})}.$$

As shown in [11, 20], the rotation of the above patch by an angle α is given by

$$\mathcal{I}^{\alpha,+}(\mathbf{i}+\Delta\mathbf{i}) = \sum_{k,q} a_{k,q}e^{-ik\alpha}\psi_{k,q}(\Delta\mathbf{i}),$$

and the reflection of that disc rotated by an angle α by

$$\mathcal{I}^{\alpha,-}(\mathbf{i}+\Delta\mathbf{i}) = \sum_{k,q} \overline{a_{k,q}}e^{-ik\alpha}\psi_{k,q}(\Delta\mathbf{i}),$$

where we used the fact that for real-valued images we have $a_{-k,q} = \overline{a_{k,q}}$ for both PSWFs and FB. Averaging over all rotations of the patch $\mathcal{I}(\mathbf{i}+\Delta\mathbf{i})$ and its reflection we get

$$\mathfrak{m}_2(k,q) = \frac{1}{L^2}\sum_{\mathbf{i}}\mathcal{I}(\mathbf{i})\left(\frac{1}{4\pi}\int_0^{2\pi}[a_{k,q}(\mathbf{i}) + \overline{a_{k,q}}(\mathbf{i})]e^{-ik\alpha}\,d\alpha\right)$$

$$= \delta_{k,0}\frac{1}{L^2}\sum_{\mathbf{i}}\mathcal{I}(\mathbf{i})a_{0,q}(\mathbf{i}),$$

---

[3]In [11], PSWFs are defined as $2\psi_{k,q}/\alpha_{k,q}$, but using the above definition simplifies the formula for the expansion coefficients.

where in the last equality we dropped the real part since both $\mathcal{I}$ and $\psi_{0,q}$ are real valued. Thus, the average power spectrum is effectively a vector. To estimate the clean power spectrum coefficients, we also expand the bias term in PSWFs. Writing

$$b_2(\Delta\mathbf{i}) = \sigma^2\delta(\Delta\mathbf{i}) = \sum_{k,q}\mathfrak{b}_2(k,q)\psi_{k,q}(\Delta\mathbf{i}),$$

the coefficients are given by

$$\begin{aligned}
\mathfrak{b}_2(k,q) &= \sigma^2\sum_{\Delta\mathbf{i}}\delta(\Delta\mathbf{i})\overline{\psi_{k,q}(\Delta\mathbf{i})} \\
&= \sigma^2\overline{\psi_{k,q}(\mathbf{0})} \\
&= \frac{\sigma^2}{\sqrt{2\pi}}R_{0,q}(0).
\end{aligned}$$

We then estimate the expansion coefficients of the clean power spectrum as

$$\widetilde{\mathfrak{m}_2}(k,q) = \mathfrak{m}_2(k,q) - \mathfrak{b}_2(k,q).$$

We expand the bispectrum as

$$m_3[\mathcal{I}](\Delta\mathbf{i}_1,\Delta\mathbf{i}_2) = \sum_{\substack{k_1,q_1 \\ k_2,q_2}}\mathfrak{m}_3(k_1,q_1;k_2,q_2)\psi_{k_1,q_1}(\Delta\mathbf{i}_1)\overline{\psi_{k_2,q_2}(\Delta\mathbf{i}_2)},$$

The expansion coefficients are then given by

$$\begin{aligned}
\mathfrak{m}_3(k_1,q_1;k_2,q_2) &= \sum_{\Delta\mathbf{i}_1,\Delta\mathbf{i}_2}m_3[\mathcal{I}](\Delta\mathbf{i}_1,\Delta\mathbf{i}_2)\overline{\psi_{k_1,q_1}(\Delta\mathbf{i}_1)}\psi_{k_2,q_2}(\Delta\mathbf{i}_2) \\
&= \frac{1}{L^2}\sum_{\mathbf{i}}\mathcal{I}(\mathbf{i})\left(\sum_{\Delta\mathbf{i}_1}\mathcal{I}(\mathbf{i}+\Delta\mathbf{i}_1)\overline{\psi_{k_1,q_1}(\Delta\mathbf{i}_1)}\right)\left(\sum_{\Delta\mathbf{i}_2}\mathcal{I}(\mathbf{i}+\Delta\mathbf{i}_2)\psi_{k_2,q_2}(\Delta\mathbf{i}_2)\right) \\
&= \frac{1}{L^2}\sum_{\mathbf{i}}\mathcal{I}(\mathbf{i})a_{k_1,q_1}(\mathbf{i})\overline{a_{k_2,q_2}(\mathbf{i})}.
\end{aligned}$$

Averaging over all rotations of $\mathcal{I}$ and its reflection, we obtain

$$\begin{aligned}
\mathfrak{m}_3(k_1,q_1;k_2,q_2) &= \frac{1}{L^2}\sum_{\mathbf{i}}\mathcal{I}(\mathbf{i})\left(\frac{1}{4\pi}\int_0^{2\pi}\left[a_{k_1,q_1}(\mathbf{i})\overline{a_{k_2,q_2}(\mathbf{i})}+\overline{a_{k_1,q_1}(\mathbf{i})}a_{k_2,q_2}(\mathbf{i})\right]e^{-i(k_1-k_2)\alpha}d\alpha\right), \\
&= \delta_{k_1,k_2}\frac{1}{L^2}\sum_{\mathbf{i}}\mathcal{I}(\mathbf{i})\Re\{a_{k_1,q_1}(\mathbf{i})\overline{a_{k_2,q_2}(\mathbf{i})}\}.
\end{aligned}$$

Thus, the bispectrum in our steerable basis $\mathfrak{m}_3(k_1,q_1;k_2,q_2)$ is block-diagonal, and is effectively a 3-tensor. Similarly to the power spectrum, we also expand the bias term in PSWFs as

$$b_3(\Delta\mathbf{i}_1,\Delta\mathbf{i}_2) = \gamma\sigma^2 Lm_1[\phi]\Big(\delta(\Delta\mathbf{i}_1-\Delta\mathbf{i}_2)+\delta(\Delta\mathbf{i}_1)+\delta(\Delta\mathbf{i}_2)\Big) = \sum_{\substack{k_1,q_1 \\ k_2,q_2}}\mathfrak{b}_3(k_1,q_1;k_2,q_2)\psi_{k_1,q_1}(\Delta\mathbf{i}_1)\overline{\psi_{k_2,q_2}(\Delta\mathbf{i}_2)},$$

where the coefficients are given by

$$\mathfrak{b}_3(k_1,q_1;k_2,q_2) = \gamma\sigma^2 Lm_1[\phi]\delta_{k_1,k_2}\left[\delta_{q_1,q_2}+\delta_{k_1,0}\frac{1}{2\pi}(\alpha_{0,q_1}+\alpha_{0,q_2})R_{0,q_1}(0)R_{0,q_2}(0)\right].$$

C Connection to volume

We derive a relation between the steered bispectrum derived in Sect. B to the volume, expanded in a suitable basis. Specifically, expand the Fourier-transformed volume as

$$\widehat{\phi}(c\mathbf{k}) = \sum_{\ell,m,s} a_{\ell,m,s} j_{\ell,s}(k) Y_{\ell,m}(\mathbf{k}/k), \quad k \le 1,$$

where $k = ||\mathbf{k}||_2$, c is the assumed bandlimit, Y_ℓ^m is the complex spherical harmonics

$$Y_{\ell,m}(\theta,\varphi) = \sqrt{\frac{2\ell+1}{4\pi} \cdot \frac{(\ell-m)!}{(\ell+m)!}} P_\ell^m(\cos\theta) e^{im\varphi},$$

where P_ℓ^m are the associated Legendre polynomials with the Condon-Shortley phase, and $j_{\ell,s}$ are normalized spherical Bessel functions given by

$$j_{\ell,s}(k) = \frac{4}{|j_{\ell+1}(u_{\ell,s})|} j_\ell(2u_{\ell,s}k),$$

where j_ℓ is the spherical Bessel function of order ℓ, $u_{\ell,s}$ is the sth positive zero of j_ℓ, and the radius satisfies $k \in [0,1/2]$ in Fourier space since $1/2$ is the Nyquist frequency [ISBI].

Then

$$\widehat{I}_\omega(ck,\theta) = \sum_{\ell,m,m',s} a_{\ell,m,s} Y_{\ell,m'}(\pi/2,0) D^\ell_{m',m}(\omega) j_{\ell,s}(k) e^{im'\theta},$$

whenever $k \le 1$. Express this in 2D PSWFs so [Eitan: I stopped here]

$$\widehat{I}_\omega(ck,\theta) = \sum_{N,n} b_{N,n} \psi_{N,n}(k,\theta),$$

where in papers the 2D PSWFs are defined as

$$\psi_{N,n}(k,\theta) = \frac{1}{\sqrt{2\pi}} R_{N,n}(k) e^{ik\theta},$$

but in Boris' code the expansion is actually performed with respect to

$$\widetilde{\psi}_{N,n}(k,\theta) = \frac{1}{2\sqrt{2\pi}} \alpha_{N,n} R_{N,n}(k) e^{ik\theta},$$

where $\alpha_{N,n}$ are the eigenvalues associated with $\psi_{N,n}$ - see Sect. **??** below.

We then get

$$b_{N,n} = \frac{1}{\sqrt{2\pi}} \int_0^{2\pi} \int_0^1 \widehat{I}_\omega(ck,\theta) R_{N,n}(k) e^{-iN\theta} k\,dk\,d\theta,$$

$$= \sum_{\ell,m,m',s} a_{\ell,m,s} [\sqrt{2\pi} Y_{\ell,m'}(\pi/2,0)] D^\ell_{m',m}(\omega) \left(\int_0^1 j_{\ell,s}(k) R_{N,n}(k) k\,dk \right) \left(\frac{1}{2\pi} \int_0^{2\pi} e^{i(m'-N)\theta}\,d\theta \right),$$

$$= \sum_{\ell \ge |N|} \sum_{m,s} a_{\ell,m,s} D^\ell_{N,m}(\omega) \beta_{\ell,s;N,n},$$

where
$$\beta_{\ell,s;N,n} = \begin{cases} \sqrt{2\pi}\, Y_{\ell,N}(\pi/2,0) \int_0^1 j_{\ell,s}(k) R_{N,n}(k) k\, dk, & \ell \geq |N|, \\ 0, & \ell < |N| \end{cases},$$

can be precomputed.

Then, back in real space,

$$I_\omega(r,\varphi) = \sum_{N,n} \widehat{\alpha}_{N,n} b_{N,n} \psi_{N,n}(r,\varphi),$$

$$= \sum_{\ell=0}^{L} \sum_{N,m=-\ell}^{\ell} \sum_{n=0}^{n_{\max}(N)} \sum_{s=1}^{S(\ell)} a_{\ell,m,s} \widehat{\beta}_{\ell,s;N,n} D_{N,m}^{\ell}(\omega) \psi_{N,n}(r,\varphi).$$

where $\alpha_{N,n}$ is the eigenvalue corresponding to the (N,n)th PSWF, $\widehat{\alpha}_{N,n} = (c/2\pi)^2 \alpha_{N,n}$, and $\widehat{\beta}_{\ell,s;N,n} = \widehat{\alpha}_{N,n} \beta_{\ell,s;N,n}$. In this notation, we assumed I_ω has bandlimit c and is concentrated in the unit ball in real space. We then consider the product

$$m_3(\boldsymbol{\ell},\boldsymbol{\ell}_2) = \frac{1}{L^2} \sum_{\mathbf{i}} \langle I_\omega[\boldsymbol{\ell}] I_\omega[\mathbf{i}+\boldsymbol{\ell}] \overline{I_\omega([\mathbf{i}+\boldsymbol{\ell}]_2)} \rangle_\omega,$$

$$= \sum_{\substack{N_1,n_1 \\ N_2,n_2 \\ N_3,n_3}} \langle b_{N_1,n_1} b_{N_2,n_2} \overline{b_{N_3,n_3}} \rangle_\omega \frac{1}{L^2} \sum_{\mathbf{i}} \psi_{N_1,n_1}[\boldsymbol{\ell}] \psi_{N_2,n_2}[\mathbf{i}+\boldsymbol{\ell}] \overline{\psi_{N_3,n_3}([\mathbf{i}+\boldsymbol{\ell}]_2)}.$$

Now,

$$\langle b_{N_1,n_1} b_{N_2,n_2} \overline{b_{N_3,n_3}} \rangle_\omega = \sum_{\substack{\ell_1,m_1,s_1 \\ \ell_2,m_2,s_2 \\ \ell_3,m_3,s_3}} a_{\ell_1,m_1,s_1} a_{\ell_2,m_2,s_2} \overline{a_{\ell_3,m_3,s_3}} \langle D_{N_1,m_1}^{\ell_1}(\omega) D_{N_2,m_2}^{\ell_2} \overline{D_{N_3,m_3}^{\ell_3}} \rangle_\omega$$

$$\times \beta_{\ell_1,s_1;N_1,n_1} \beta_{\ell_2,s_2;N_2,n_2} \overline{\beta_{\ell_3,s_3;N_3,n_3}},$$

and [Tamir's note on Kam's bispectrum]

$$\langle D_{N_1,m_1}^{\ell_1}(\omega) D_{N_2,m_2}^{\ell_2} \overline{D_{N_3,m_3}^{\ell_3}} \rangle_\omega = (-1)^{N_3+m_3} \begin{pmatrix} \ell_1 & \ell_2 & \ell_3 \\ N_1 & N_2 & -N_3 \end{pmatrix} \begin{pmatrix} \ell_1 & \ell_2 & \ell_3 \\ m_1 & m_2 & -m_3 \end{pmatrix},$$

and since $\begin{pmatrix} \ell_1 & \ell_2 & \ell_3 \\ m_1 & m_2 & m_3 \end{pmatrix} = 0$ unless $m_1 + m_2 + m_3 = 0$ and $|\ell_1 - \ell_2| \leq \ell_3 \leq \ell_1 + \ell_2$, we conclude that

$$\langle b_{N_1,n_1} b_{N_2,n_2} \overline{b_{N_3,n_3}} \rangle_\omega = \delta_{N_3,N_1+N_2} \sum_{\substack{\ell_1,m_1,s_1 \\ \ell_2,m_2,s_2 \\ s_3}} \sum_{\ell_3=|\ell_1-\ell_2|}^{\min(L,\ell_1+\ell_2)} a_{\ell_1,m_1,s_1} a_{\ell_2,m_2,s_2} \overline{a_{\ell_3,m_1+m2,s_3}}$$

$$\times (-1)^{N_1+N_2+m_1+m_2} \begin{pmatrix} \ell_1 & \ell_2 & \ell_3 \\ N_1 & N_2 & -N_1-N_2 \end{pmatrix} \begin{pmatrix} \ell_1 & \ell_2 & \ell_3 \\ m_1 & m_2 & -m_1-m_2 \end{pmatrix}$$

$$\times \beta_{\ell_1,s_1;N1,n_1} \beta_{\ell_2,s_2;N_2,n_2} \overline{\beta_{\ell_3,s_3;N1+N2,n_3}}.$$

20

Finally, we expand

$$m_3(\boldsymbol{\ell}, \boldsymbol{\ell}_2) = \sum_{k, q_1, q_2} \mathfrak{m}_3(k, q_1, q_2) \psi_{k, q_1}(\boldsymbol{\ell}) \overline{\psi_{k, q_2}(\boldsymbol{\ell}_2)},$$

where we only include the block-diagonal terms in the expansion. Defining

$$\Psi_{\ell, N, s}[\boldsymbol{\ell}] = \sum_{n=0}^{n_{\max}(N)} \beta_{\ell, s; N, n} \psi_{N, n}[\boldsymbol{\ell}],$$

the final formula reads

$$\mathfrak{m}_3(k, q_1, q_2) = \sum_{\substack{\ell_1, m_1, s_1 \\ \ell_2, m_2, s_2 \\ s_3}} \sum_{\ell_3 = |\ell_1 - \ell_2|}^{\min(L, \ell_1 + \ell_2)} a_{\ell_1, m_1, s_1} a_{\ell_2, m_2, s_2} \overline{a_{\ell_3, m_1 + m_2, s_3}}$$

$$\times (-1)^{m_1 + m_2} \begin{pmatrix} \ell_1 & \ell_2 & \ell_3 \\ m_1 & m_2 & -m_1 - m_2 \end{pmatrix}$$

$$\times \sum_{N_1 = -\ell_1}^{\ell_1} \sum_{N_2 = -\ell_2}^{\ell_2} (-1)^{N_1 + N_2} \begin{pmatrix} \ell_1 & \ell_2 & \ell_3 \\ N_1 & N_2 & -N_1 - N2 \end{pmatrix} \frac{1}{L^2} \sum_{\mathbf{i}} \Psi_{\ell_1, N_1, s_1}[\boldsymbol{\ell}] \rho_{\ell_2, N_2, s_2}^{(k, q_1)}[\boldsymbol{\ell}] \overline{\rho_{\ell_3, N_1 + N_2, s_3}^{(k, q_2)}[\boldsymbol{\ell}]},$$

where

$$\rho_{\ell, N, s}^{(k, q)} = \int_{\boldsymbol{\ell}} \Psi_{\ell, N, s}([\mathbf{i} + \boldsymbol{\ell}]) \overline{\psi_{k, q}(\boldsymbol{\ell})}.$$

In practice, the last line of the above expression for $\mathfrak{m}_3(k, q_1, q_2)$ is precomputed, and both the integration over $\mathbf{i}$ and over $\boldsymbol{\ell}$ is performed on the grid of the images in the dataset, to match the integration performed on the actual images.

C.1   The power spectrum

The power spectrum is easier to derive directly in Fourier space, to avoid integration of shifted prolates against centered ones. The average power spectrum in Fourier space can be derived from Kam's original formula [Kam, 1980; Eq. 10] by setting $\mathbf{k}_1 = \mathbf{k}_2$ to obtain

$$\langle |\widehat{I}_\omega(k, \theta)|^2 \rangle_\omega = \frac{1}{4\pi} \sum_{\ell, m} \left| \sum_s a_{\ell, m, s} j_{\ell, s}(k) \right|^2 = \frac{1}{4\pi} \sum_{\substack{\ell, m \\ s_1, s2}} a_{\ell, m, s_1} \overline{a_{\ell, m, s_2}} j_{\ell, s_1}(k) j_{\ell, s_2}(k),$$

where we used the fact that the normalized spherical Bessel functions $j_{\ell, s}$ are real. To expand the above in 2D PSWFs, we write

$$\langle |\widehat{I}_\omega(k, \theta)|^2 \rangle_\omega = \sum_q \mathfrak{m}_2(q) \psi_{0, q}(k),$$

and conclude that

$$\mathfrak{m}_2(q) = \frac{\sqrt{2\pi}}{4\pi} \sum_{\substack{\ell, m \\ s_1, s_2}} a_{\ell, m, s_1} \overline{a_{\ell, m, s_2}} \int_0^1 j_{\ell, s_1}(k) j_{\ell, s_2}(k) R_{0, q}(k) k \, dk.$$

C.2 The mean

Since the Fourier transformed volume is given by

$$\widehat{V}(k,\theta,\varphi) = \sum_{\ell,m,s} a_{\ell,m,s} Y_{\ell,m}(\theta,\varphi) j_{\ell,s}(k),$$

since $j_{\ell,s}(0) = 0$ unless $\ell = 0$, and since $Y_{0,0}(\theta,\varphi) = \frac{1}{\sqrt{4\pi}}$, we conclude that

$$m_1[\phi] = \widehat{V}(\mathbf{0}) = \frac{1}{\sqrt{4\pi}} \sum_s a_{0,0,s} j_{0,s}(0).$$

$$C_2^{(q)} = \int_0^1 j_{\ell,s_1}(k) j_{\ell,s_2}(k) R_{0,q}(k) k \, dk$$

$$C_3^{(k,q_1,q_2)} \ell_1, m_1, s_1; \ell_2, m_2, s_2; \ell_3, s_3) := (-1)^{m_1+m_2} \left(\begin{array}{ccc} \ell_1 & \ell_2 & \ell_3 \\ m_1 & m_2 & -m_1 - m_2 \end{array} \right)$$

$$\times \sum_{N_1=-\ell_1}^{\ell_1} \sum_{N_2=-\ell_2}^{\ell_2} (-1)^{N_1+N_2} \left(\begin{array}{ccc} \ell_1 & \ell_2 & \ell_3 \\ N_1 & N_2 & -N_1 - N2 \end{array} \right) \frac{1}{L^2} \sum_{\mathbf{i}} \Psi_{\ell_1,N_1,s_1}[\boldsymbol{\ell}] \rho_{\ell_2,N_2,s_2}^{(k,q_1)}[\boldsymbol{\ell}] \overline{\rho_{\ell_3,N_1+N_2,s_3}^{(k,q_2)}[\boldsymbol{\ell}]},$$

and

$$\rho_{\ell,N,s}^{(k,q)} = \int_{\boldsymbol{\ell}} \Psi_{\ell,N,s}([\mathbf{i}+\boldsymbol{\ell}]) \overline{\psi_{k,q}(\boldsymbol{\ell})}.$$

C.3 Implementation details

To implement the above formula, we precompute the quantities

$$W(\ell_1,\ell_2,\ell_3,m_1,m_2) = (-1)^{m_1+m_2} \left(\begin{array}{ccc} \ell_1 & \ell_2 & \ell_3 \\ m_1 & m_2 & -m_1 - m_2 \end{array} \right),$$

and

$$B^{(k,q_1,q_2)}(\ell_1,\ell_2,\ell_3,s_1,s_2,s_3) = \sum_{N_1=-\ell_1}^{\ell_1} \sum_{N_2=-\ell_2}^{\ell_2} W(\ell_1,\ell_2,\ell_3,N_1,N_2) \frac{1}{L^2} \sum_{\mathbf{i}} \Psi_{\ell_1,N_1,s_1}[\boldsymbol{\ell}] \rho_{\ell_2,N_2,s_2}^{(k,q_1)}[\boldsymbol{\ell}] \overline{\rho_{\ell_3,N_1+N_2,s_3}^{(k,q_2)}[\boldsymbol{\ell}]},$$

so in each iteration of the optimization we compute

$$\mathfrak{m}_3(k,q_1,q_2) = \sum_{\substack{\ell_1,\ell_2,\ell_3 \\ m_1,m_2 \\ s_1,s_2,s_3}} W(\ell_1,\ell_2,\ell_3,m_1,m_2) B^{(k,q_1,q_2)}(\ell_1,\ell_2,\ell_3,s_1,s_2,s_3) \times$$

$$a_{\ell_1,m_1,s_1} a_{\ell_2,m_2,s_2} \overline{a_{\ell_3,m_1+m_2,s_3}}.$$

The Wigner $3j$ symbols are computed from the Racah formula

$$\left(\begin{array}{ccc} \ell_1 & \ell_2 & \ell_3 \\ m_1 & m_2 & -m_3 \end{array} \right) = \delta_{m_3,m_1+m_2} (-1)^{\ell_1-\ell_2+m_3} \sqrt{\Delta(\ell_1,\ell_2,\ell_3)}$$

$$\times \prod_{i=1}^{3} \sqrt{(\ell_i - m_i)!(\ell_i + m_i)!} \times \sum_t \frac{(-1)^t}{x(t)},$$

where

$$x(t) = t!(\ell_3 - \ell_2 + t + m_1)!(\ell_3 - \ell_1 + t - m_2)!(\ell_1 + \ell_2 - \ell_3 + t)!(\ell_1 - t - m_1)!(\ell_2 - t + m_2)!,$$

the sum is over all integer t for which the arguments in the factorials in $x(t)$ are all nonnegative, and

$$\Delta(\ell_1, \ell_2, \ell_3) = \frac{(\ell_1 + \ell_2 - \ell_3)!(\ell_1 - \ell_2 + \ell_3)!(-\ell_1 + \ell_2 + \ell_3)!}{(\ell_1 + \ell_2 + \ell_3 + 1)!}.$$

D   Noisy micrograph moments

We now suppose that the micrograph is perturbed by additive white Gaussian noise, so we observe $\widetilde{\mathcal{I}} = \mathcal{I} + \varepsilon$ where $\varepsilon \overset{\text{iid}}{\sim} \mathcal{N}(0, \sigma^2 I)$. We proceed to derive $\lim_{N \to \infty} m_2[\widetilde{\mathcal{I}}]$, $m_3[\widetilde{\mathcal{I}}]$. For simplicity of notation, we shall use vectorized indices $\mathbf{i} = (i, j)$.

D.1   Expansion in PSWFs

In practice, we compute the moments of our noisy micrograph in a product basis of 2D prolates, so we need to derive the expansion coefficients of the above bias terms in these functions for debiasing.

To this end, writing (in the continuous case again)

$$\delta(\boldsymbol{\ell} - \boldsymbol{\ell}_2) = \sum_{k, q_1, q_2} \mathfrak{d}(k, q_1, q_2) \psi_{k,q_1}(\boldsymbol{\ell}) \overline{\psi_{k,q_2}(\boldsymbol{\ell}_2)},$$

we get

$$\mathfrak{d}(k, q_1, q_2) = \int_{\boldsymbol{\ell}, \boldsymbol{\ell}_2} \delta(\boldsymbol{\ell} - \boldsymbol{\ell}_2) \overline{\psi_{k,q_1}(\boldsymbol{\ell}_1)} \psi_{k,q_2}(\boldsymbol{\ell}_2)$$

$$= \int_{\boldsymbol{\ell}_2} \overline{\psi_{k,q_1}(\boldsymbol{\ell}_2)} \psi_{k,q_2}(\boldsymbol{\ell}_2)$$

$$= \delta_{q_1, q_2}.$$

Similarly, writing

$$\delta(\boldsymbol{\ell}_1) = \sum_{k, q_1, q_2} \mathfrak{d}^{(1)}(k, q_1, q_2) \psi_{k,q_1}(\boldsymbol{\ell}_1) \overline{\psi_{k,q_2}(\boldsymbol{\ell}_2)},$$

we get

$$\mathfrak{d}^{(1)}(k, q_1, q_2) = \int_{\boldsymbol{\ell}_1, \boldsymbol{\ell}_2} \delta(\boldsymbol{\ell}_1) \overline{\psi_{k,q_1}(\boldsymbol{\ell}_1)} \psi_{k,q_2}(\boldsymbol{\ell}_2)$$

$$= \overline{\psi_{k,q_1}(\mathbf{0})} \int_{\boldsymbol{\ell}_2} \psi_{k,q_2}(\boldsymbol{\ell}_2)$$

$$= \delta_{k,0} R_{0,q_1}(0) \int_0^1 R_{0,q_2}(r) r \, dr$$

$$= \delta_{k,0} \frac{\alpha_{0,q_2}}{2\pi} R_{0,q_1}(0) R_{0,q_2}(0),$$

where we used the fact that $R_{0,q}$ satisfies

$$\frac{\alpha_{0,q}}{2\pi} R_{0,q}(r) = \int_0^1 R_{0,q}(\rho) J_0(cr\rho)\rho\,d\rho,$$

where J_k is the Bessel function of the first kind, and that $J_0(0) = 1$. A similar derivation applies to $\delta(\boldsymbol{\ell}_2)$.

Thus, in terms of the prolate expansion coefficients, our bias formulas become

$$\widetilde{\mathfrak{m}}_3(k, q_1, q_2) = \mathfrak{m}_3(k, q_1, q_2) + \sigma^2 m_1[\widetilde{\mathcal{I}}] \left[\delta_{q_1,q_2} + \delta_{k,0} \frac{1}{2\pi}(\alpha_{0,q_1} + \alpha_{0,q_2}) R_{0,q_1}(0) R_{0,q_2}(0) \right].$$

Similarly, for the power spectrum we get

$$\widetilde{\mathfrak{m}}_2(q) = \mathfrak{m}_2(q) + \sigma^2 \frac{1}{\sqrt{2\pi}} R_{0,q}(0).$$